Supporting Information for

A Universal Growth Method for High Quality Phase-Engineered Germanium Chalcogenide Nanosheets

Junyu Qu[a,b,†], Chenxi Liu [a,b,†], Muhammad Zubair[a,b,†], Zhouxiaosong Zeng[b], Bo Liu[a,b], Xin Yang[a,b], Ziyu Luo[a,b], Xiao Yi[a,b], Ying Chen[a,b], Shula Chen[a,b,‡], and Anlian Pan[a,b,‡].

AFFILIATIONS

[1]Key Laboratory for Micro-Nano Physics and Technology of Hunan Province, College of Materials Science and Engineering, Hunan University, Changsha, Hunan 410082, P.R. China

[2]Hunan Institute of Optoelectronic Integration, Hunan University, Changsha, 410082, China

‡.Authors to whom correspondence should be addressed: shuch@hnu.edu.cn and anlian.pan@hnu.edu.cn.

† These authors contributed equally to this work

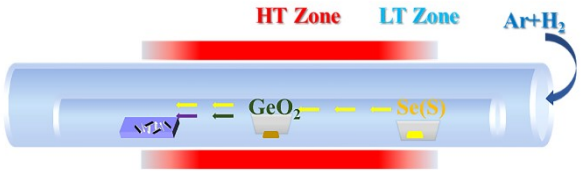

Fig. S1. Schematic diagram of the experimental setup and the controllable growth process of Germanium chalcogenide.

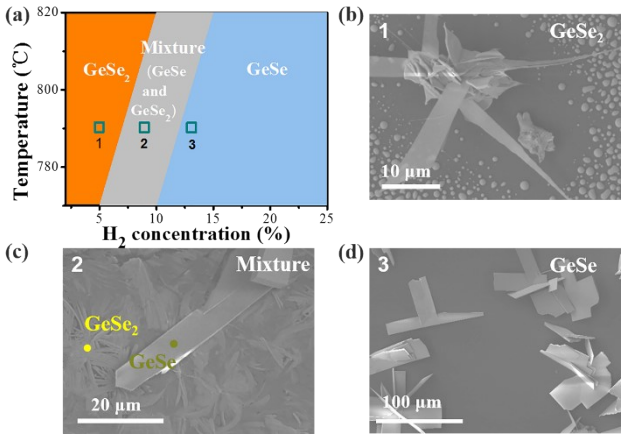

Fig. S2. (a) Phase diagram for the growth of GeSe and $GeSe_2$. (b-d) Typical growth results under the growth conditions marked with 1, 2 and 3 in (a), respectively

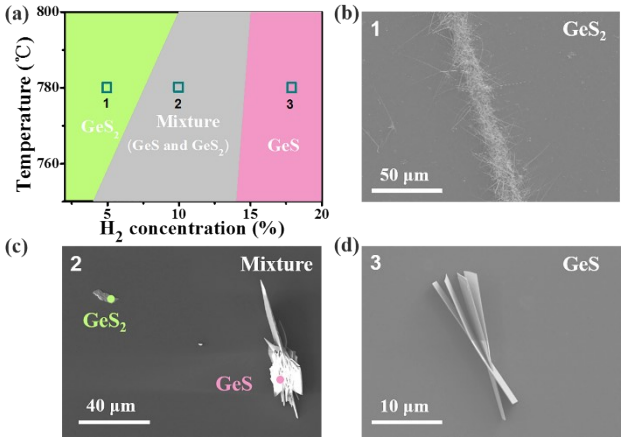

Fig. S3. (a) Phase diagram for the growth of GeS and GeS_2. (b-d) Typical growth results under the growth conditions marked with 1, 2 and 3 in (a), respectively

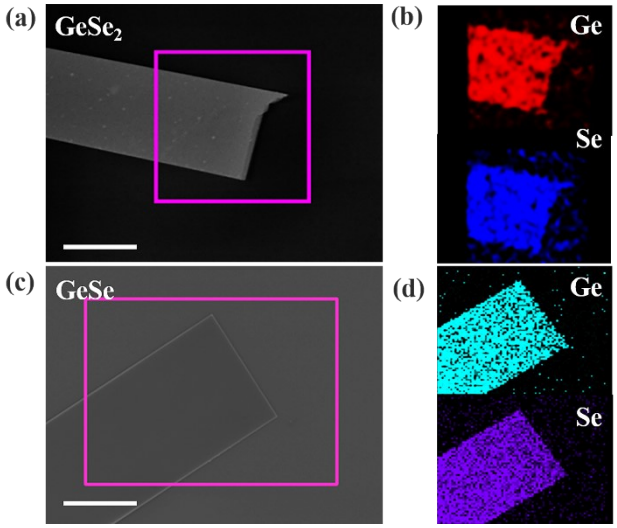

Fig. S4. SEM images and the element mapping of GeSe and $GeSe_2$. (a)SEM image of $GeSe_2$. Scale bar is 5 μm. (b) elemental mapping in the pink rectangle region of the $GeSe_2$. (c) SEM image of GeSe. Scale bar is 5 μm. (d) elemental mapping in the pink rectangle region of the GeSe.

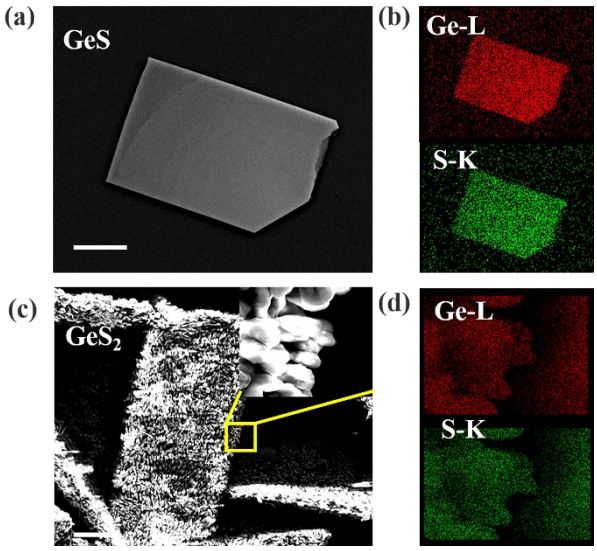

Fig. S5. SEM images and the element mapping of GeSe and $GeSe_2$. (a)SEM image of $GeSe_2$. Scale bar is 5 μm. (b) elemental mapping in the pink rectangle region of the $GeSe_2$. (c) SEM image of GeSe. Scale bar is 5 μm. (d) elemental mapping in the pink rectangle region of the GeSe images and the element mapping of GeSe and $GeSe_2$.

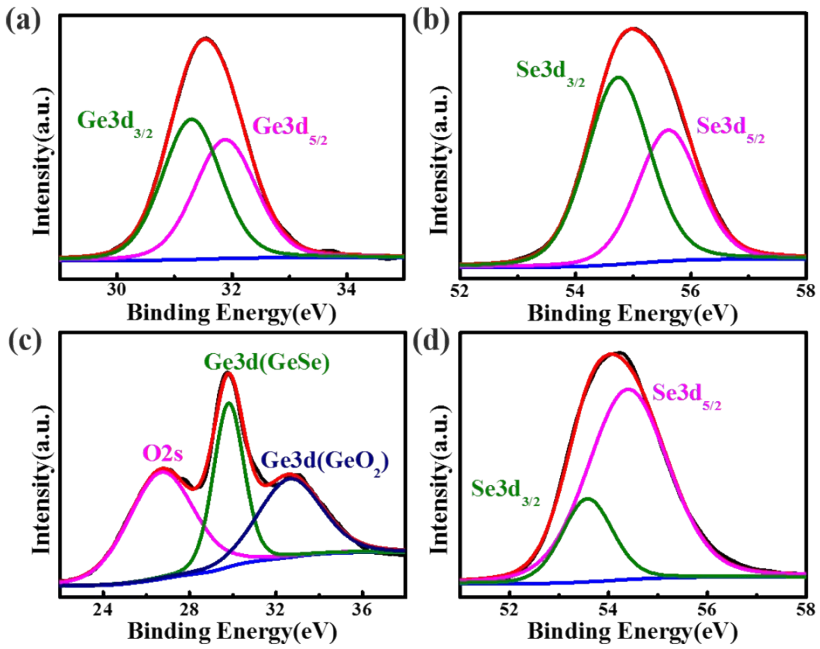

Fig. S6. XPS spectra of $GeSe_2$ (a,b) and GeSe (c,d). The core line signals of Ge 3d and Se 3d located at 31.5 eV and 55.0 eV for $GeSe_2$, while they are situated at 30.0 eV (Ge 3d) and 54.1 eV (Se 3d) for GeSe.

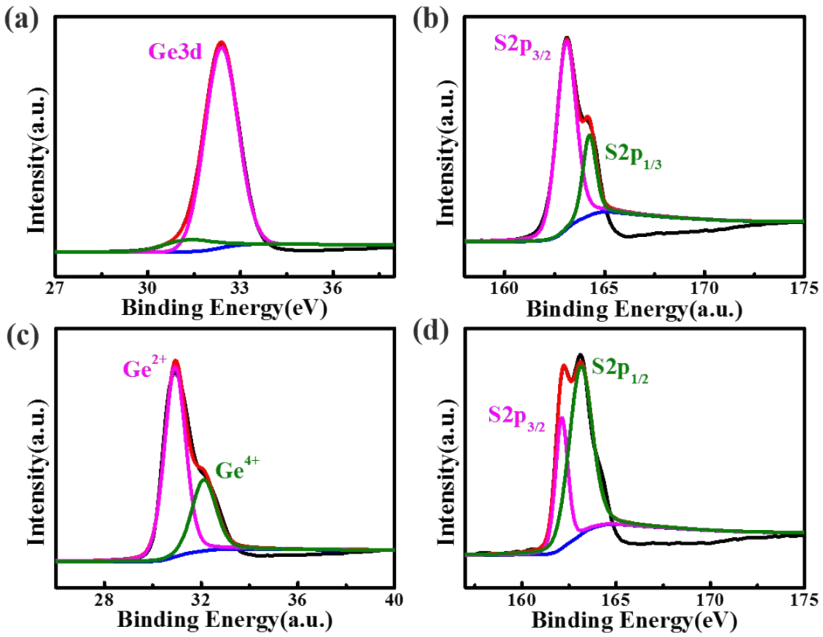

Fig. S7. XPS spectra of GeS_2 (a,b) and GeS (c,d). There are peaks of GeS_2 located at 32.3 eV (Ge 3d, GeS_2), 163.1 eV (S $p_{3/2}$, GeS_2) and 164.2 eV (S $2p_{1/3}$, GeS2) in Fig. S7(a) and S7(b). Figure S7(c) and S7(d) show the binding energy of Ge^{2+} (30.9 eV), Ge^{4+} (32.1 eV), S $2p_{3/2}$ (162.1 eV) and S $2p_{1/2}$ (163.1 eV) in GeS.

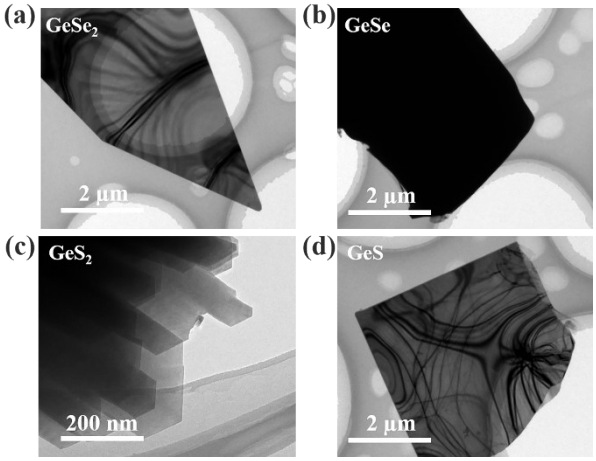

Fig. S8. Low-magnification TEM image of $GeSe_2$(a), GeSe(b), GeS_2(c) and GeS(d).

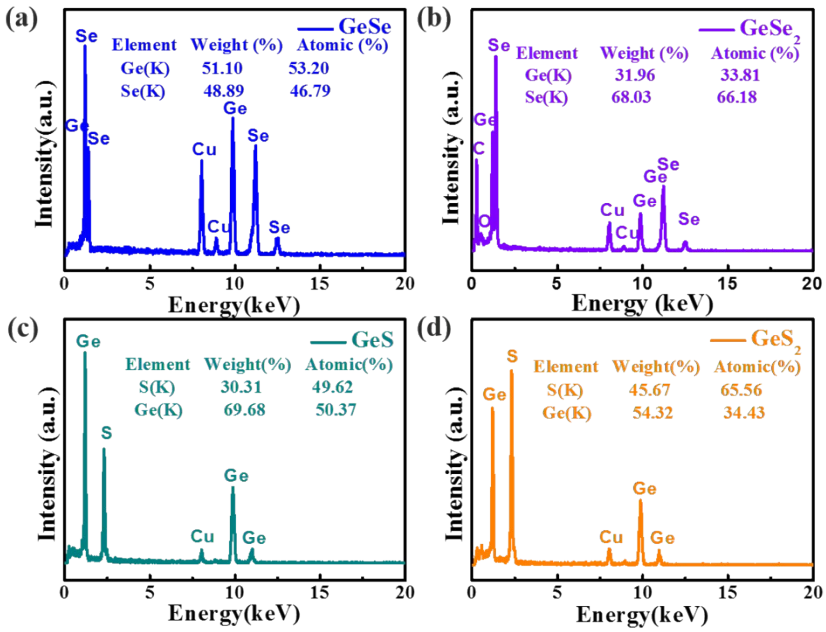

Fig. S9. EDS spectra of GeSe(a), $GeSe_2$(b), GeS(c) and GeS_2(d). The EDS spectrum of GeSe (a) shows that the Ge/Se ratio is ~1:1. The EDS spectrum of $GeSe_2$ (b) shows that the Ge/Se ratio is ~1:2. The EDS spectrum of GeS (c) shows that the Ge/S ratio is ~1:2. The EDS spectrum of GeS_2 (d) shows that the Ge/S ratio is ~1:2.

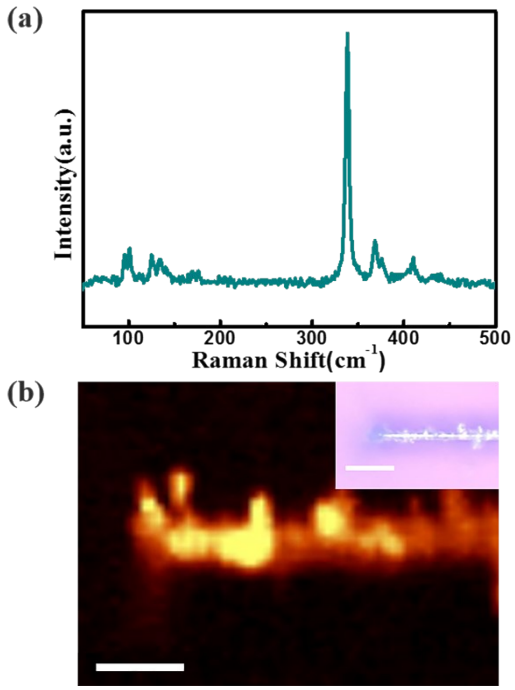

Fig. S10. Raman feature of GeS_2. (a) Raman spectrum of GeS_2. (b) Raman mapping of GeS_2.The inset is the corresponding optical image. Scale bar is 5 μm.

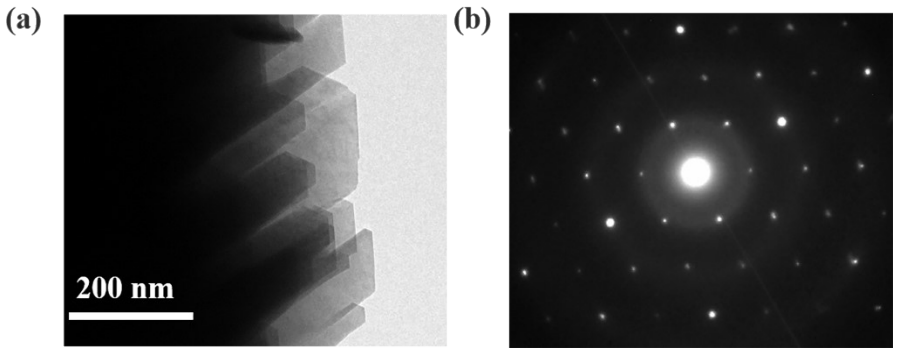

Fig. S11. Low-magnification TEM image of GeS_2(a) and the corresponding selected area electron diffraction pattern(b). Because of the instability of the grown GeS_2 under high energy electron beam, the high-resolution TEM image is unavailable.

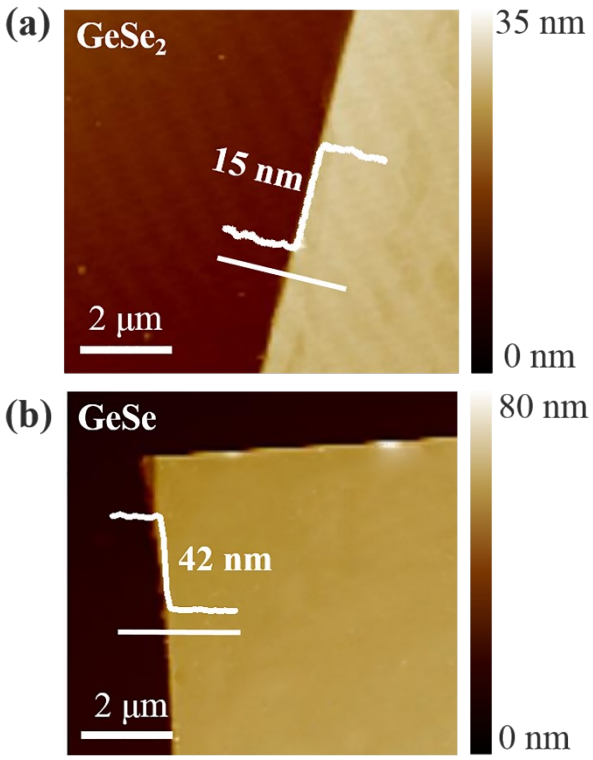

Fig. S12. AFM image of GeSe and $GeSe_2$. (a)AFM image of $GeSe_2$. (b)AFM image of GeSe.

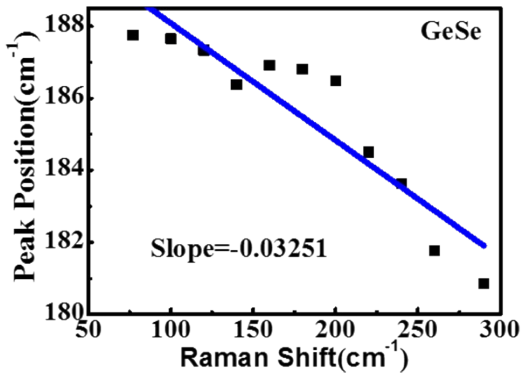

Fig. S13. Temperature-dependence of the phonon peak position of the A^3_g mode at 150 cm^{-1} of GeSe nanobelt.

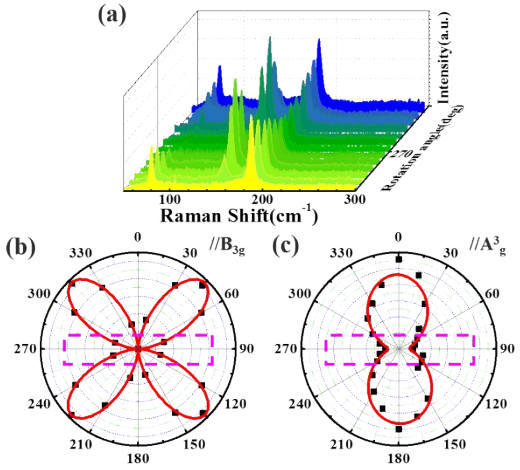

Fig. S14. (a) Angle - dependent Raman spectra of GeSe at angle ranging from 180º to 360º. (b) Angle-resolved Raman scattering intensities of B_{3g} modes under parallel configureuration. (c) Angle-resolved Raman scattering intensities of A^3_g modes under parallel configureuration.

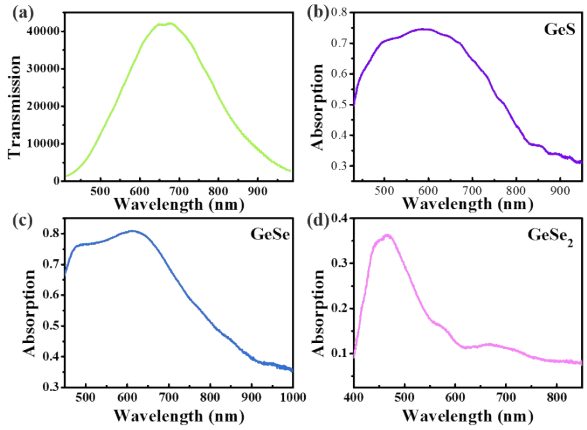

Fig. S15. The absorption measurements of the grown germanium chalcogenide nanosheets. (a) The transmission of the transparent glass sheet. (b-d) The absorption spectra of GeS (b), GeSe (c) and $GeSe_2$ (d)

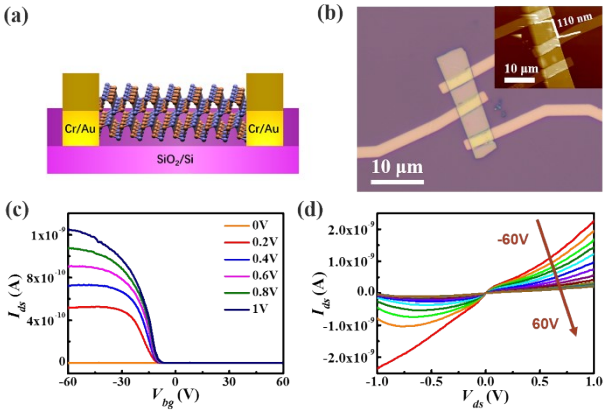

Fig. S16. (a) Schematic structure of the GeS photodetector. (b) Optical image of the device. Upper right is the corresponding AFM image, scale bar is 20 μm. (c) I_{ds}-V_{bg} transfer curves at various V_{ds} values. (d) I_{ds}-V_{ds} output characteristics of the device at gate voltage varying from -60 to 60 V.

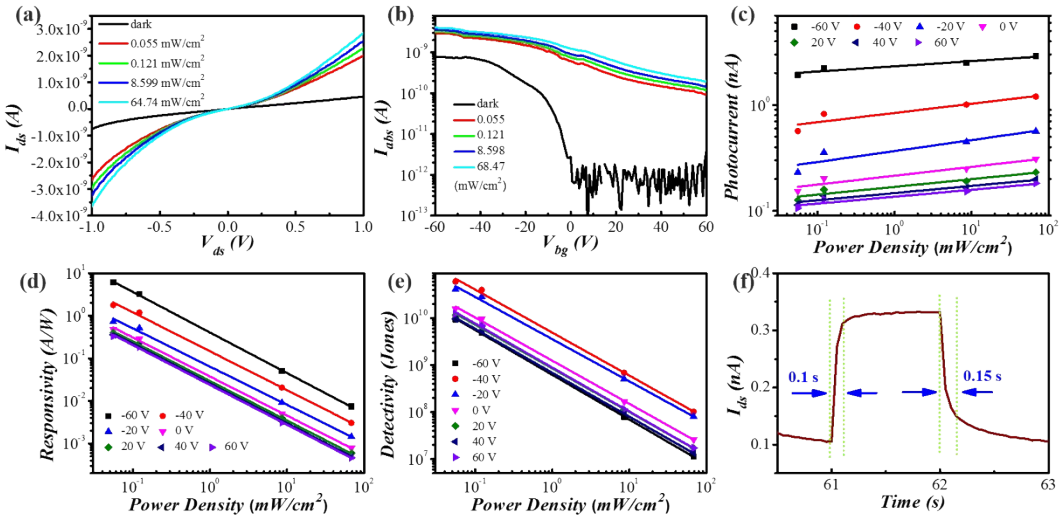

Fig. S17. Optoelectronic characteristics of GeS-based device. (a) Output curves of GeS under different 520 nm irradiation intensities at V_{bg}= -60 V. (b) Transfer curves in the dark and under diverse 520 nm laser intensities at V_{ds} = 1 V. (c-d) Irradiation power dependence of photocurrent (c), photoresponsivity (d) and detectivity (e) of GeS at V_{ds}=1 V. (f) The on/off switching of the GeS. The calculated photoresponsivity and dectectivity of GeS are 0.005 $cm^2V^{-1}s^{-1}$, 6.1 A/W and 9.3×10^9 Jones.

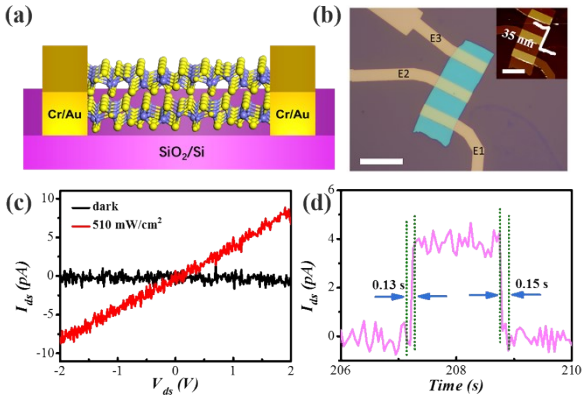

Fig. S18. Optoelectronic characteristics of $GeSe_2$-based device. (a) Schematic structure of the $GeSe_2$ photodetector. (b) Optical image of the device. Upper right is the corresponding AFM image, scale bar is 20 μm. (c) I-V curves of $GeSe_2$ under dark and 405 nm irradiation. (d) The on/off switching of the $GeSe_2$. The calculated photoresponsivity and dectectivity of $GeSe_2$ are 1.5×10^{-6} A/W and 6.2×10^{4} Jones.

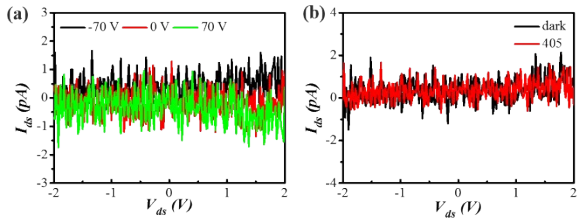

Fig. S19. Optoelectronic characteristics of GeS_2-based device. (a)Output curves of GeS_2 under various gate voltages. (b) I-V curves of GeS_2 under dark and 405 nm irradiation.

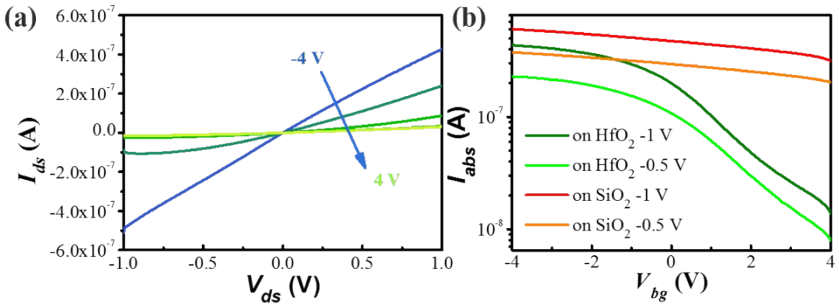

Fig. S20. (a) Output curves of GeSe on HfO_2/Si and SiO_2/Si substrate. (b) Transfer curves of GeSe on HfO_2/Si and SiO_2/Si substrate.

Table. S1. Comparison of grown GeSe-based photodetector performance with other reported 2D semiconductors prepared by CVD

Material	Fabrication Mathod	Spectral region	Responsivity [A W^{-1}]	Detectivity [Jones]	Rise time [ms]	Ref
$SnSe_2$	CVD	NIR	1.9	-	-	22
SnS_2	CVD	visible	261	1.9×10^{10}	20	46
MoS_2	CVD	visible	0.057	10^{10}	0.07	51
$MoSe_2$	CVD	visible	93.7	-	400	53
WS_2	CVD	visible	9.2×10^{-5}	-	5.3	54
ReS_2	CVD	visible	16.14	-	105	55
GaTe	CVD	UV-visible	0.03	-	54	56
HfS_2	CVD	UV-visible	2.8×10^{3}	-	55	49
HfS_3	CVD	visible	0.11	-	<400	57
ZrS_3	CVD	visible	0.53	-	<400	57
In_2Se_3	CVD	visible	578	6×10^{12}	20	52
$ReS_{2(1-x)}Se_{2x}$	CVD	Visible-NIR	0.25	-	15	50
GeSe	CVD	visible	9.3×10^{3}	-	48	23
GeSe	CVD	visible	1.16×10^{5}	9.82×10^{12}	11	This work